Oriented intra-granular bubble transport due to coupling of pinned bubble growth and dislocation climb

L. Noirot, L. Verma, P. Maugis

Oriented intra-granular bubble transport due to coupling of pinned bubble growth and dislocation climb

L. Noirot[a], L. Verma [b], P. Maugis[c]

[a] *CEA, DES/IRESNE/DEC Saint-Paul-lez-Durance, 13108, France*
[b] *CEA, DES/IRESNE/DEC Saint-Paul-lez-Durance, 13108, France*
[c] *Aix Marseille Univ, Univ Toulon, CNRS, IM2NP, Marseille, France*

Abstract

The intra-granular fission gas release during post-irradiation annealing tests cannot be predicted by the effective diffusion theory ($D_{eff} = \frac{b}{b+g} D_{Xe}$). In this case, the equilibrium between trapping (g) and re-solution (b) is completely shifted in favor of the trapping, as dynamic re-solution due to fission spikes does not exist anymore after irradiation. Several alternative scenarios involving bubble movement emerged to explain the observed fission gas release. The purpose of our work is to assess these scenarios using simulation. In a previous article, it was demonstrated that neither the movement of bubbles in a vacancy gradient, nor the Brownian movement of bubbles, nor the combination of them, could explain the large fission gas release obtained during post-irradiation annealing in our reference experiment. This demonstration was performed using a mesoscale model, called BEEP, where individual bubbles are described, along with the diffusion of vacancies from each bubble to the other, as well as from the free surface. In this paper, we extend the BEEP model to assess the role of dislocations in interaction with highly pressurized bubbles. It is concluded that a mechanism of dislocation climb coupled with the growth of highly pressurized pinned bubbles may explain the large intra-granular fission gas release in annealing conditions.

Keywords: Fission gas, Nuclear fuel, Modeling, Intra-granular bubble, Meso-scale, Dislocation, Bubble transport

Email address: laurence.noirot@cea.fr (L. Noirot)

L. Verma's present affiliation: PSN-RES/SAM/LETR, Institut de Radioprotection et de Sûreté Nucléaire, 13115, St. Paul les Durance, France

1. Introduction

Understanding fission gas behavior during nuclear reactor operation is very important for optimal utilization of fuel rod. This is because fission gases generated during irradiation in a nuclear fuel cause macroscopic phenomena like Fission Gas Release (FGR) and swelling in the fuel, which can affect the proper functioning of the fuel rod. FGR from the fuel increases the pressure in the fuel rod plenum, subjecting the cladding to additional stress, and reduces the thermal conductivity of the fuel-cladding gap, causing the fuel operating temperature to increase. Due to their low solubility in UO_2, fission gases also precipitate into highly pressurized bubbles causing the swelling of the fuel. Swelling contributes to the fuel-cladding interaction, again exposing the cladding to higher stress and temperature conditions and eventually affecting its operational life.

In order to understand fission gas behavior, in-pile as well as out-of-pile measurements are carried out in the nuclear fuel. However, carrying out measurements in a fuel under irradiation (in-pile) can be difficult due to uncontrollable environment. Post-irradiation annealing (out-of-pile) tests are carried out to obtain data on FGR under controlled and monitored environment. During post-irradiation annealing tests, one of the interesting issues has been the transport of intra-granular gas to the grain surface, as it is found to be significant on the contrary to the effective diffusion theory [**?**], which would predict no intra-granular gas release at all. Indeed, the effective diffusion coefficient is equal to $D_{eff} = \frac{b}{b+g} D_{Xe}$, where b and g are the re-solution and trapping probabilities per second, respectively, and D_{Xe} is the intrinsic diffusion coefficient of the gas. In the absence of fission and if Xe is considered as insoluble in UO_2, the re-solution probability, b, is nil. In other words, atomic gas is immediately trapped by the intra-granular bubbles, which are present in abundance [**?**].

Several mechanisms for the transport of intra-granular gas atoms outside the grain have been proposed. Thermal resolution of gas atoms was invoked [**?**] [**?**] but was progressively ruled out based on both solution energy calculations [**?**] [**?**] and bubble size distribution analysis [**?**].

Inhibition of gas precipitation into over-pressurized bubbles was proposed by Ronchi [**?**]. In order to take into account the stress field in the vicinity of an over pressurized bubble, it is necessary to use the chemical potential gradient to calculate the xenon flux. The chemical potential of xenon depends on the trace of the stress tensor at the considered location. Around a spherical

bubble at very high pressure, the trace of the stress tensor is constant, radial compression being counter-balanced by the tensile stresses in the tangential directions. Therefore, Ronchi's approach does not seem convincing.

Other scenarios have to consider bubble movement. By studying the release of volatile fission products at high temperature, Germain [**?**] [**?**] showed that a good prediction could be obtained by assuming that any species in gaseous form is transported to the grain boundary with the same kinetics as xenon. This can be considered as an indication that species in gaseous form and xenon are transported by the motion of the same bubbles. Evans [**?**] suggested that the rapid transport of gas atoms could be due to the movement of intra-granular bubbles containing the gas in a vacancy concentration gradient. However, in a preceding paper [**?**], we demonstrated that neither the movement of bubbles in a vacancy gradient, nor the Brownian movement of bubbles, nor the combination of them, could explain the large fission gas release obtained during post-irradiation annealing in our reference experiment (65% of Fission Gas Release (FGR) for 3 hours of isothermal annealing at 1600°C [**?**]).

In this article, we focus on a mechanism coupling the transport of pinned bubbles on edge dislocations and the climb of these dislocations. This mechanism involves the generation and diffusion of vacancies along the core of the dislocation, and their trapping by the pinned bubbles. In the literature, similar phenomena are addressed in [**?**] [**?**].

The organization of the paper is as follows: In Section 2 the coupled bubble transport and dislocation climb mechanism is presented as well as the theoretical formulation of the resulting dislocation velocity. The implementation of this mechanism in BEEP model [**?**] [**?**] is explained in Section 3. Section 4 presents a verification test. Then a realistic case calculation is presented and discussed in Section 5 and the conclusion and perspectives are presented in Section 6.

2. Mechanism of coupled dislocation climb and pinned bubble movement and growth

The idea behind this mechanism is that vacancy production is possible on an edge dislocation and that diffusion of vacancies is much faster along a dislocation than in the bulk. Producing vacancies on edge dislocations would be the easiest way for the fuel to swell when most of the bubbles are inside the grains and pinned on these dislocations. As these produced

vacancies would finally contribute to the intra-granular bubble growth, the result would be a pressure decrease inside these bubbles. A flow of vacancies along the dislocation towards the bubble implies an inverse flow of Uranium atoms from the bubble surface. These new Uranium atoms would be added to the half plane(s) of atoms, which would lead to a climb of the dislocation. If we add the hypothesis that bubbles remain linked to the dislocations, the result would be an oriented movement of the pinned bubbles, with the dislocations. This mechanism is illustrated in Fig. 1. Fig. 2 shows the vacancy generation, diffusion along the dislocation core, and trapping by the bubble.

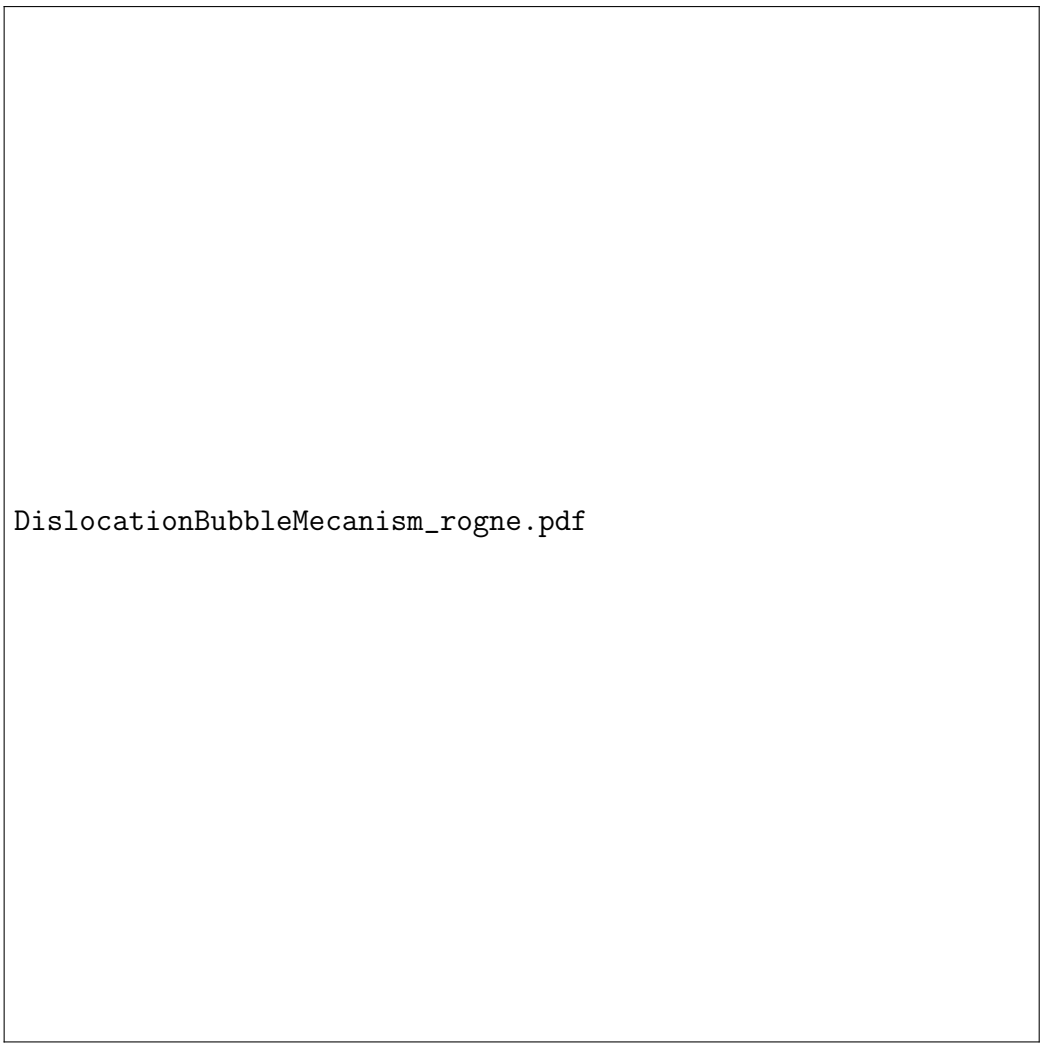

Figure 1: Coupled bubble movement and dislocation climb.

Figure 2: Vacancy generation, diffusion along the dislocation core, and trapping by the bubble.

2.1. Formulation

The idea for the formulation of the growth of a bubble pinned on a dislocation was adopted from the approach of Speight and Beere [**?**] for the vacancy potential and void growth on grain boundaries. They demonstrated how cavity growth proceeds by absorption of vacancies generated on the grain boundaries. They related the total work exerted on the solid with the chemical potential of vacancies. The implementation of this approach to a dislocation with pinned bubbles is presented below. The final formulation consists in the Eq. 1, which gives the velocity with which the dislocation moves and the Eq. 2 which gives the growth kinetics of the bubbles pinned on the same dislocation.

$$v_d = \frac{12D^*}{kT}\Omega^{4/3}\frac{(P_i - \frac{2\gamma}{R_i} - P_{ext})L_{tot}}{\sum_i L_i^3} \tag{1}$$

$$\frac{d\sum_{bubble\,i} V_{bi}}{dt} = wL_{tot}v_d \tag{2}$$

D^* is the coefficient of vacancy diffusion on the dislocation (m^2/s) multiplied by the equilibrium vacancy concentration on the dislocation, $x_{v_d}^{eq}$, (fraction/site), k is the Boltzmann constant, T is the temperature in Kelvin, P_i is the internal pressure of the pinned bubble in Pascal, $\frac{2\gamma}{R_i}$ is the Laplace pressure, P_{ext} is the external pressure on the system (typically the atmospheric pressure for usual annealing tests), L_i is the length of the segment of the dislocation that is between bubble 'i-1' and bubble 'i', both pinned on it, and L_{tot} is the total length of the dislocation (including the bubble diameters) as presented on Fig.3. Finally w is the width of the dislocation core and V_{bi} is the volume of bubble 'i'.

The reasoning leading to these equations uses the concept of chemical potential of vacancies on the dislocation (see Appendix A for this), and the vacancy source term β on the dislocation. Here the hypothesis done is that there is a uniform vacancy source term β that takes place in the volume of the dislocation core and that these vacancies continuously diffuse and are trapped by the bubble.

From the Fick's law, we have the diffusion equation at steady state as:

$$\frac{D_{v_d}}{\Omega}\nabla^2 x_{v_d} + \beta = 0 \tag{3}$$

where $\frac{x_{v_d}}{\Omega}$ is a concentration in vac/m^3 (x_{v_d} is a vacancy concentration in fraction of sites), and β is a source term in $vac/m^3/s$.

There is a link between the chemical potential of vacancies along the dislocation and their concentration (See Appendix A):

$$\mu = E_{v_d} + kTln(x_{v_d}) \tag{4}$$

The vacancy concentration at equilibrium on the dislocation corresponds to $\mu = 0$ as:

$$x_{v_d}^{eq} = exp\left(-\frac{E_{v_d}}{kT}\right)$$

Finally, the chemical potential can be represented as:

$$\mu \;\; = \;\; kTln\left(\frac{x_{v_d}}{x_{v_d}^{eq}}\right)$$

In the case where we consider that x_{v_d} is in general close to $x_{v_d}^{eq}$, and because $ln(1+x) \approx x$ when $x << 1$,

$$\mu = kTln\left(\frac{x_{v_d}^{eq} + \delta x_{v_d}}{x_{v_d}^{eq}}\right) \approx kT\left(\frac{\delta x_{v_d}}{x_{v_d}^{eq}}\right)$$

So, the Laplacian of μ is:

$$\nabla^2\mu = \frac{kT}{x_{v_d}^{eq}}\nabla^2 x_{v_d} \tag{5}$$

because $\nabla^2 x_{v_d} = \nabla^2 \delta x_{v_d}$, since $x_{v_d}^{eq}$ is constant in space (uniform temperature).

So, using Eq. 5, the Fick's law (Eq. 3) can be transformed into:

$$\nabla^2\mu + \frac{\beta\Omega kT}{D_{v_d}x_{v_d}^{eq}} = 0$$

which can be written as:

$$\nabla^2\mu + \frac{\beta\Omega kT}{D^*} = 0 \tag{6}$$

where $D^* = D_{v_d} \times x_{v_d}^{eq}$

Now, we can get the average vacancy chemical potential of the segment L_i (See Fig.4).

Integrating eq. 6 twice, with $\mu(x = L_i/2) = 0$, and $\vec{\nabla}\mu(x = 0) = 0$ gives us:

$$\mu = -\frac{\beta\Omega kT}{2D^*}\left[x^2 - \left(\frac{L_i}{2}\right)^2\right]$$

Integrating the above in the limits of 0 to $L_i/2$:

$$\int_0^{\frac{L_i}{2}} \mu dx = -\frac{\beta\Omega kT}{2D^*}\int_0^{\frac{L_i}{2}}\left[x^2 - \left(\frac{L_i}{2}\right)^2\right]dx$$

and then dividing by $L_i/2$, we get the average vacancy chemical potential for i, as:

$$\overline{\mu_i} = \frac{\beta\Omega kT}{12D^*}L_i^2 \tag{7}$$

We define Δt, as the time needed for the dislocation to climb one layer ($\Omega^{1/3}$). During this time, vacancies are created in the dislocation segments (of volume $\Omega^{1/3} * w * L_i$) at a rate of β and are replaced by the atoms coming from the bubble surfaces.

At the same time, an additional volume is provided to the bubbles because the crystal goes apart around the bubbles when the dislocation climbs. This volume is $\sum_i \Omega^{1/3} w d_i$, where d_i is the diameter of the bubble 'i'.

The flux of vacancies arriving at the bubble 'i' per second is:

$$\beta\Omega^{1/3} w\left(\frac{L_i}{2} + \frac{L_{i+1}}{2}\right)$$

The net work done on the solid, W, is:

$$W = \sum_{bubble\ i}\left[\underbrace{\beta\Delta t\Omega^{1/3} w\left(\frac{L_i}{2} + \frac{L_{i+1}}{2}\right)\Omega}_{\text{(I)}} + \underbrace{\Omega^{1/3} w d_i}_{\text{(II)}}\right]\left(P_i - \frac{2\gamma}{R_i}\right)\underbrace{-P_{ext}\Omega^{1/3} w\left(\sum_i L_i + \sum_i d_i\right)}_{\text{(III)}} \tag{8}$$

The term (I) represents the volume change of the bubble due to the flux of vacancies and term (II) represents the additional volume change. The term (III) is the resistant work done on the system by the external pressure.

In time Δt, $\frac{\Omega^{1/3} w \sum_i L_i}{\Omega}$ vacancies have been generated in the volume $\Omega^{1/3} w \sum_i L_i$. This means:

$$\beta \Delta t * \Omega^{1/3} w \sum_i L_i = \frac{\Omega^{1/3} w \sum_i L_i}{\Omega}$$

which gives us

$$\beta \Delta t = \frac{1}{\Omega} \tag{9}$$

Using the expression for $\beta \Delta t$ from Eq.9 in term (I) in Eq. 8, defining the sum of dislocation segment lengths and bubble diameters as L_{tot}, and considering that all the bubbles on the same dislocation are equilibrated (i.e., same P_i and R_i), we get the net work done in Eq.8 as:

$$W = \Omega^{1/3} w \left(P_i - \frac{2\gamma}{R_i} - P_{ext} \right) L_{tot} \tag{10}$$

The central idea is that the net work done on the solid is used to generate the vacancies on the dislocation and can be related to the average vacancy chemical potential (in J/site) as:

$$W = \sum_i \overline{\mu_i} \frac{\Omega^{1/3} w L_i}{\Omega}$$

Using the expression for $\overline{\mu_i}$ from Eq.7 and the net work done from Eq.10 and rearranging for β, we get:

$$\beta = \frac{12 D^*}{kT} \frac{\left(P_i - \frac{2\gamma}{R_i} - P_{ext} \right) L_{tot}}{\sum_i L_i^3} \quad in\ vacancy/m^3/s \tag{11}$$

Moreover, for the dislocation velocity, we have $velocity = \frac{distance\ climbed}{time}$, so:

$$v_d = \frac{\Omega^{1/3}}{\Delta t}$$

and from Eq. 9, we can get $1/\Delta t$. So the dislocation velocity is defined in terms of β as:

$$v_d = \beta \Omega^{4/3}$$

which gives finally the Eq. 1.

In the previous reasoning, the crystal is considered as cubic for the sake of simplicity. The link with the real UO_2 crystallography can be done through w. What is important to respect is n_c, the number of U atoms that must be added to the atomic plane(s) behind the edge dislocation per length $\Omega^{1/3}$ of dislocation, to make this dislocation climb of $\Omega^{1/3}$. These added plane(s) of atoms behind the dislocation can be visualized in blue on Fig. 5. In the model, we have to take $w = n_c \times \Omega^{1/3}$. The higher w is, the faster the bubbles grow for the same dislocation velocity, and the faster their inner pressure drops.

Following the analysis from the thesis of Le Prioux [**?**], the only dislocation loops likely to grow are those which do not present a stacking fault. They form two classes. The first ones have a Burgers vector in the $< 110 >$ direction and include two extra planes of atoms. The second ones have a Burgers vector in the $< 111 >$ direction and include three extra planes of atoms. In the first case, $n_c = 4^{\frac{1}{3}}/\sqrt{2} = 1.122$. The width of the dislocation $w = 4^{\frac{1}{3}}/\sqrt{2} \times \Omega^{1/3} = \frac{\sqrt{2}}{2} \times a$ is equal to the magnitude of the Burgers vector (a is the FCC UO_2 mesh parameter). In the second case, $n_c = 4^{\frac{1}{3}}\sqrt{3} = 2.749$. The width of the dislocation $w = 4^{\frac{1}{3}}\sqrt{3} \times \Omega^{1/3} = \sqrt{3} \times a$ is also equal to the magnitude of the Burgers vector. In the two cases, the equality of w to the Burgers vector magnitude is due to the fact that the atomic density in the volume added (formed by two planes in the first case and by three planes in the second case) is 1 atom / Ω, which is consistent with the absence of stacking fault, and to the fact that the Burgers vector is perpendicular to the added plane(s). The experimental work of Onofri [**?**] (pp 111-112) showed that the prismatic loops or the edge dislocation lines with a Burgers vector $< 110 >$ were the most common. That is why we took the width $w = 1.122 \times \Omega^{1/3}$, in the following.

With these formulations, dislocation climb continues as long as the bubbles on the dislocations are over-pressurized. A situation where the dislocation is highly decorated with bubbles (small $\sum_i L_i^3$) is also favorable for the dislocation climb as well as an easy diffusion of vacancies along the dislocation (pipe diffusion) and/or an easy vacancy generation on the dislocation (which depends on E_{v_d}). Usually, solid precipitates that are pinned on a dislocation tend to slow it. Therefore, the fact that bubbles may be the driving force for dislocation climb may be surprising. However, one has to consider that highly over-pressurized gas bubbles are very uncommon objects in material science, and their interaction with dislocations a quite unknown field.

3. Implementation of coupled dislocation/bubble behavior in the BEEP model

BEEP model has been presented in two previous papers [**?**] [**?**]. This code has been designed to deal with the particular problem of bubble movement in annealing conditions. BEEP is a spatialized model, in the sense that every bubble is represented, with its own position, size, content... The main assumptions adopted in the model before the introduction of dislocations were the following [**?**]:

- We assume that the simulation starts after gas has been trapped in the bubbles. Therefore, the Xe gas atoms are present inside the cavities and not in the solid. We also think that the irradiation defects largely annihilate with the temperature and the few that remain would be trapped in the extended defects. This is why we only consider thermal defects in the model.
- The UO_2 fuel is modeled as a mono-crystal containing spherical cavities.
- Each UO_2 is considered as an "atom" and Schottky defects as "vacancies" in the description of the model.
- Only vacancies are considered as point defects in the model for the present study. Indeed the auto-interstitial U or the anti-Schottky defect have large formation energies and can hardly be produced thermally.
- Bubbles are assumed to be spherical and remain so. This assumption is justified for the intra-granular bubbles at high temperature.
- No irradiation is considered in the model, i.e., it is applicable for annealing tests.
- Surfaces - surfaces of the bubbles and surface of the grain - are sources or sinks of vacancies.
- The model is developed to function in both 2-D and 3-D.

In order to add dislocations to the model:

- We assume that the solid contains a few edge dislocations, represented as straight lines.

- Any bubble that touches a dislocation is and will remain pinned on the dislocation.
- Any bubble pinned on a dislocation has its center on the dislocation line.
- Pinned bubbles move with the dislocation. They also may move by another mechanism but only along directions that are compatible with their status of pinned bubbles. For example, a pinned bubble (of center $y = y_0$, $x = x_0$, $z = z_0$ on a dislocation line defined by ($y = y_0$, $x = x_0$) and moving along the x direction by Δx during the time step keeps the possibility of moving randomly, for instance, in the z direction. So, at the end of the time step, its center coordinates will be $y = y_0$, $x = x_0 + \Delta x$, and $z \neq z_0$.
- Bubbles pinned on a dislocation may coalesce with any other bubble. If the other bubble is not pinned, the resulting bubble will be pinned.
- If bubble 1 (pinned on dislocation 1) and bubble 2 (pinned on dislocation 2) coalesce, the resulting bubble will be pinned on the dislocation of the largest bubble.
- For simplicity, all the bubbles that are pinned on the same dislocation are equilibrated (in volume and gas content). This is the condition for a straight dislocation line to remain straight.
- The vacancies generated on the dislocation line diffuse only along the dislocation core, and not in the solid. This is a simplification suggested by the fact that the diffusion is probably much faster along the dislocation than in the bulk.
- The volume change of pinned bubbles is calculated as for other bubbles, including in addition the contribution of the vacancy flux coming along the dislocation.
- BEEP is designed to represent a volume with periodic conditions or a rectangular parallelepiped, with periodic conditions along the y- and z-axis, symmetry condition for $x = 0$ and a free surface on the last side (exactly, a so called "flat bubble"). For the dislocation studies, we used the second kind of domain only, and the dislocations were parallel to the free surface.

3D analysis was mandatory to assess the impact of the dislocation climb on bubbles, because in 2D a dislocation would have swept systematically the entire represented bubbles. However, 3D calculation increases the computational elapsed time dramatically. That is why parallelization has been introduced to the BEEP model, for the computation of vacancy diffusion in the bulk.

Dislocations were added to the BEEP model in the form of new objects "dislocation" that are mainly defined by:

- The dislocation ID,
- The unitary vector $\vec{u}$ along the dislocation (See Fig. 5),
- The point P_d, intersection of the box sides and the dislocation line that verifies $\vec{P_dC} \cdot \vec{u} > 0$, C being the center of the domain,
- The target point, $P_{d_{target}}$, that defines the position of the dislocation at the end of the time step,
- The unitary vector $\vec{v}$ that defines the direction for the dislocation climb,
- The total length of the dislocation in the box,
- The source term of vacancy on the dislocation, β,
- The dislocation velocity, v_d
- The vector of so-called "dislocation items", which are other objects, detailed below,
- Two variables AtomsOnGrainSidePrevious and AtomsOnGrainSideCurrent: These are the counterparts of the creation of vacancies in all the dislocation segments plus the simultaneous creation of voids in the pinned bubbles of the dislocation, at the beginning and end of the time step. In the BEEP model, before the introduction of dislocations, a procedure of verification of the atom balance had been developed, as a way to check the code. In a real sample, when vacancies are generated on a dislocation the total sample swells. The atoms counterparts are, in a way, the atoms that are beyond the former envelope of the solid. For a time step, they are the atoms of the blue volume in Fig. 1. Because of the periodic conditions in the y and z directions, it is not possible to

represent the envelope of the solid, which would be perpendicular to y- and z-axis. Instead, we count these atoms through these two variables, for each dislocation. It can also be seen as the atoms that would be added to the extra plane(s) of atoms behind the dislocation line since the beginning of the calculation. The procedure of verification of the atom balance has been changed in order to take these quantities into account.

- A variable "pinningOrCoalescenceOccured" that is equal to 0 or 1 ; 1 means that the pinning of a new bubble occurred, or that a bubble of the dislocation coalesced: in these case, the number of 'dislocations items' that constitute the decorated dislocation changes.

Figure 3: Schematic view of a pinned bubble, dislocation segment, and dislocation core dimensions.

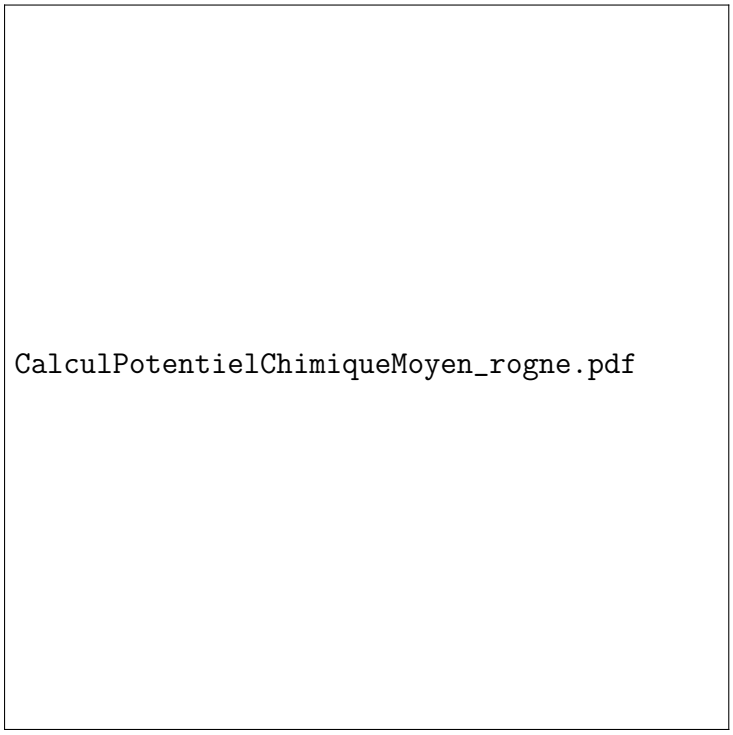

Figure 4: Geometry used for the average vacancy chemical potential calculation.

Figure 5: Definition of a dislocation line in BEEP model.

An object "dislocation item", is simply the collection of a dislocation segment, characterized by its length, L_i, a bubble (bubble 'i'), and the position of their first intersection, P_i, when the dislocation line is followed in the direction of the unitary vector $\vec{u}$. A vector of such "dislocation items" defines completely the succession of segments and pinned bubbles that constitute the decorated dislocation (see Fig. 6).

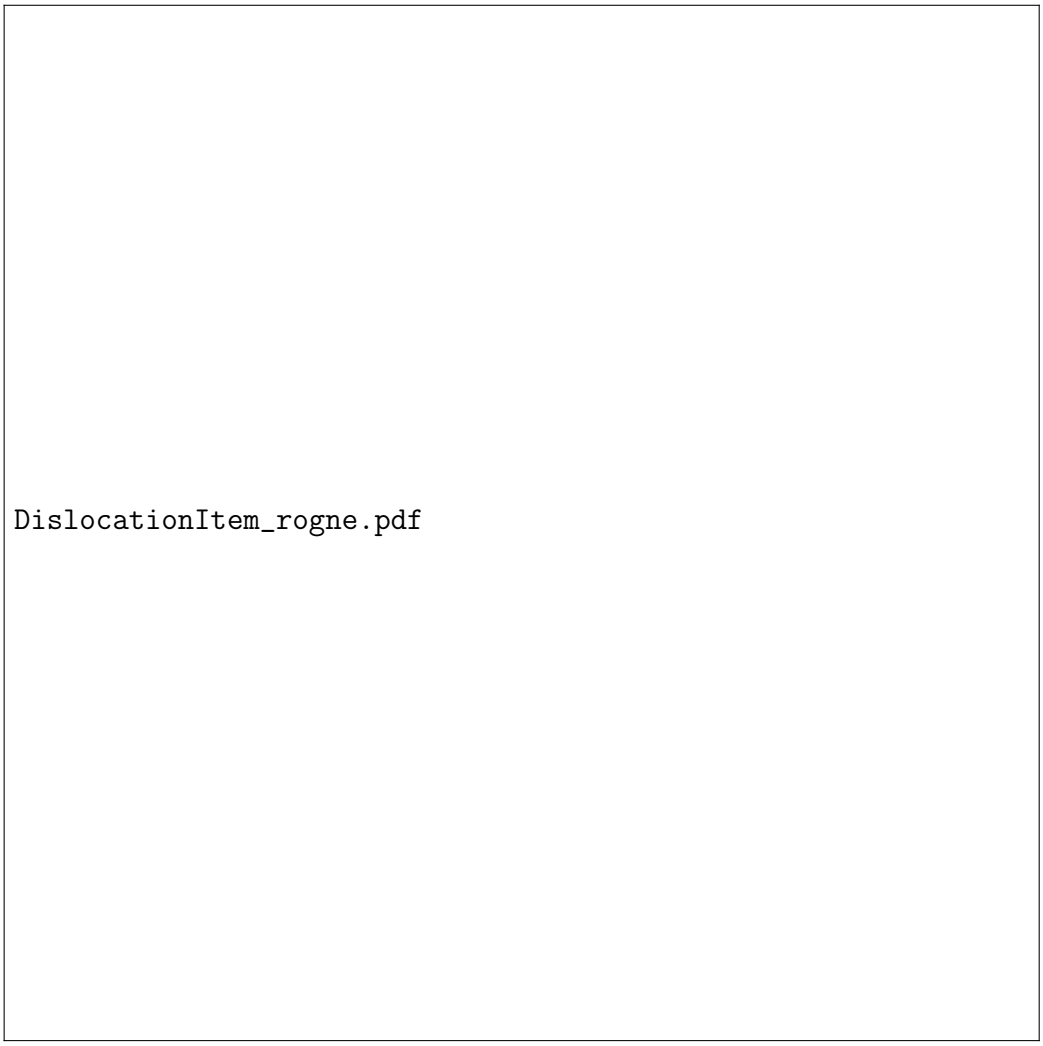

Figure 6: Definition of a dislocation item in BEEP model.

Associated with this geometrical description, different methods allow the calculation of the vacancy fluxes for each dislocation segment, the dislocation

velocity, and the occurrence of a new bubble pinning. For the latter, the position of the dislocation and each bubble are determined at the end of the time step (as if no interaction happened), and then the different objects (bubbles and dislocation) are supposed to move in a straight line during the time step, with displacements proportional to the time. As soon as a moving bubble and the moving dislocation come in contact on their trajectory during the time step, the bubble is pinned on the dislocation. So, for the remaining duration within the time step, the bubble continues its displacement, but with the constraint of being pinned to the dislocation. For example, in Fig 6, the new pinned bubble center will have the same x and z as the dislocation at the end of the time step, and the y calculated for its end of time step position without interaction. In order to track dislocation and bubble encounter, geometrical methods as "calculate the distance of the bubble center to the dislocation" were also added.

Besides, pinned bubbles remain bubbles, so the development made previously in BEEP to check and deal with the coalescence of bubbles are still valid and active.

Fig. 7 shows the modifications done on BEEP algorithm to take into account the dislocations.

4. Verification

The first test case that we performed with the new model is presented in Fig. 8 [**?**]. There was only one vertical dislocation, which went through bubble 1, at the beginning of the calculation. We had placed four other bubbles on the way of the dislocation. The purpose of this test was to verify how "free bubbles " and a pinned bubble coalesce, check the impact on the dislocation velocity, test the impact of bubble growth with the vacancy flux coming from the dislocation line on the inner pressure of the pinned bubble, and see whether the dislocation would finally reach the free surface or not, and evaluate the time taken by the entire process.

We considered a domain with a size of $128\,nm \times 64\,nm \times 64\,nm$ and a grid size of h = 4 nm and an exterior region with a free surface. The length of the exterior region was 10 nm. The five bubbles were of radius 5 nm and the volume per atom of gas was taken equal to Ω, the atomic volume, in each bubble. In this case, no bulk vacancy diffusion, nor random movement of the bubble was considered. The direction of the climb of the dislocation was towards the free surface. Since the diffusion of vacancies on the dislocation is

not known, we considered it as a parameter and took the value for $D^* = 3.93$ 10^{-18} m^2/s in order to have a velocity of dislocation so that it can eventually move out of the surface on the right. The simulation was carried out for a time of 2178 s at the isothermal annealing temperature of 1600°C.

Dislocations are not represented on the Paraview films that we generate, because the visualization was done in terms of the solid fraction, RS, of each cell (or voxel), with RS = 1 (red) for solid cells, RS = 0 (black) for empty cells and RS in between 0 and 1 (and colors going from cold colors to hot colors) for the interface cells. For the 2D case, this representation was very convenient. However, in 3D, with such a rule, the bubble are completely embedded in red areas and are not visible in practice. So, in order to see the bubbles, a filter was added to the visuals, which only included the values of RS strictly less than 1. This removed the solid region (red) from the visual and the interface cells and the empty cells of the bubbles could be visualized clearly.

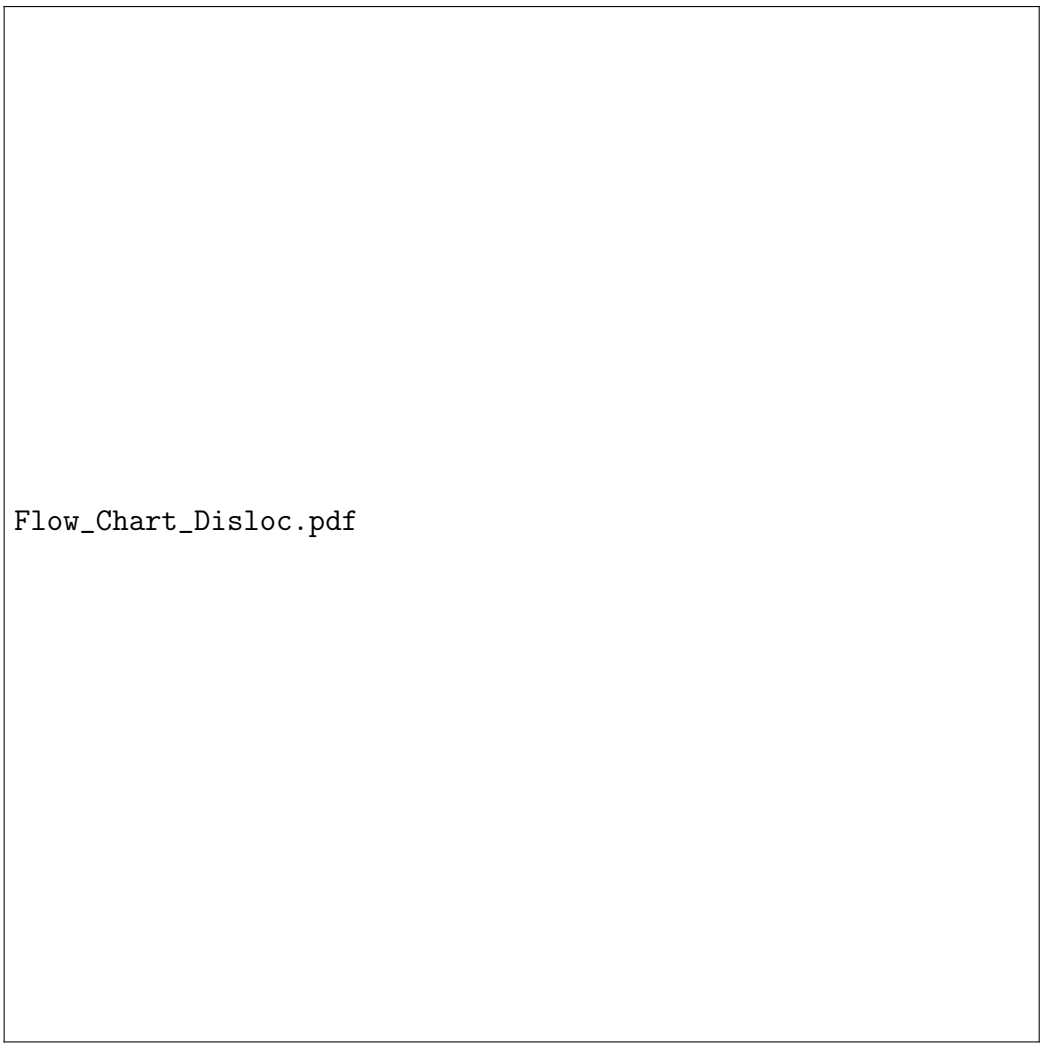

Figure 7: Incorporation of dislocations into BEEP Model.

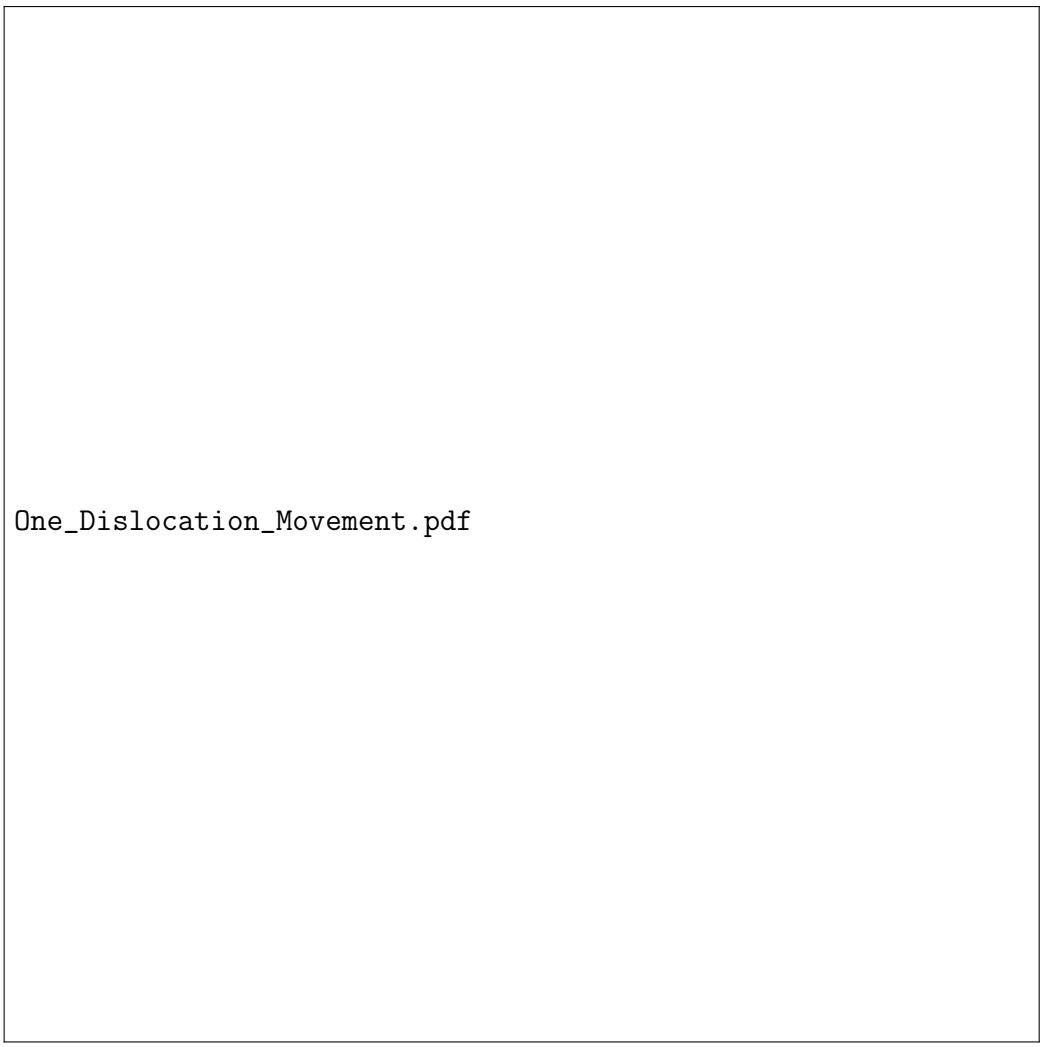

Figure 8: Bubble movement via Dislocation climb mechanism.

Bubble 1 gas content and velocity, which is also the dislocation velocity, are presented in Fig.9 and the bubble 1 volume in Fig. 10. Bubble 2, 3, 4 and 5 are in turn captured by the dislocation, making bubble 1 grow. In between such coalescence events, the dislocation velocity decreases, because as vacancies generated on the dislocation are added to the bubble, its inner pressure decreases and becomes closer to the external pressure, causing the driving force to seize. When bubble 1 encounters another bubble, there is a sudden increase in the dislocation velocity as the Bubble 1, pinned to the dislocation, acquires the gas atoms and the volume of the coalesced bubble. Indeed, the coalescence of Bubble 1 and Bubble 2, for instance, increases the internal pressure of the resulting Bubble 1 because Bubble 1 had already begun to relax its inner pressure with the vacancies coming from the dislocation, while Bubble 2 had its high inner pressure unchanged. There is also the effect of the new radius of the resulting Bubble 1, which causes the Laplace pressure ($\frac{2\gamma}{R_i}$) to decrease. Both the effects make the effective pressure ($P_i - \frac{2\gamma}{R_i}$) and the over-pressurization of Bubble 1 to increase just after coalescence. So, the dislocation velocity increases instantly and continues on the downward curve thereafter. Bubble 1 ends touching the free surface at 1980 s, which leads to the coalescence of bubble 1 with the exterior (considered as a "flat bubble" in BEEP), and fission gas release.

Figure 9: Evolution of the velocity of the dislocation and pinned bubble gas content with time.

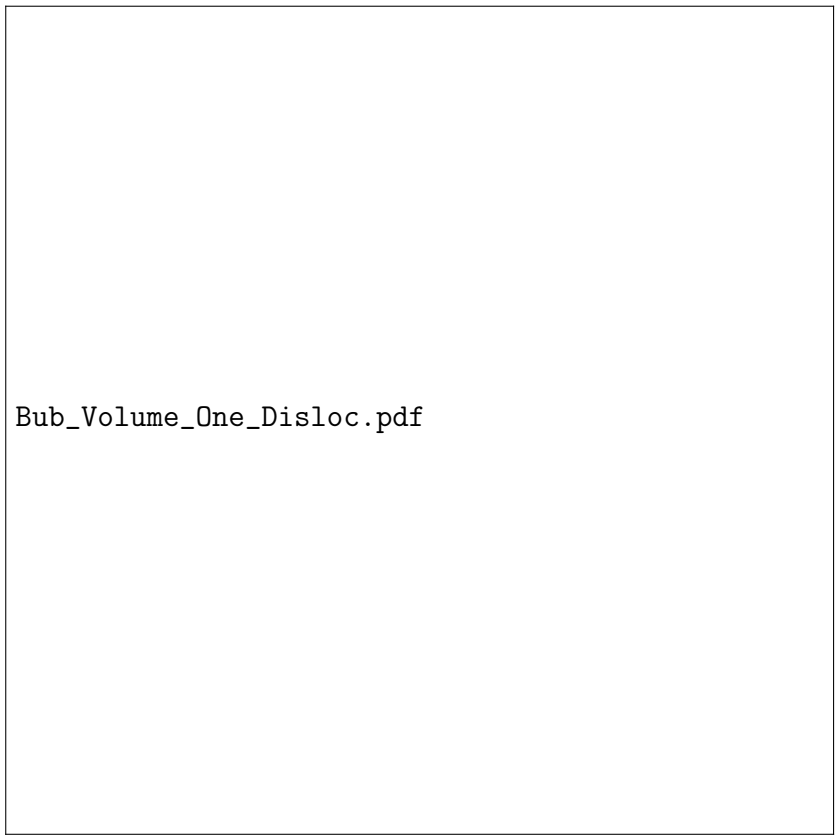

Figure 10: Volume of the pinned bubble on dislocation.

Since the model behaves as expected, a more realistic case was calculated and is detailed in the following section.

5. Results and discussion

In this section, we present a case using the dislocation/bubble coupled transport and the comparison of the FGR to that from experimental data of an annealing test.

5.1. Fission gas release values from experiments for comparison

We compare the values of FGR obtained from the model presented above to the results from the experiments presented in the thesis of Valin [**?**]. She used a pellet of UO_2 fuel (enriched to 4.5% of U-235) from a PWR which had been irradiated for one cycle. The mean grain size was 11 μm. At the end of the irradiation, the burnup was 14.2 GWd/t_U and there was nearly no FGR. The fragments of the whole pellet were annealed for 3 hours at $1600°C$. During the annealing, the specimen was swept by helium at a flow rate of 60 cm^3/min. The Kr^{85} release was continuously monitored by a spectrometer. In addition, the total quantity released was also determined by analyzing cold traps. The fraction of FGR was found to be ∼65%.

However, this FGR cannot be compared directly to the FGR obtained with the model. As explained in [**?**], the reason is twofold: firstly, the value of FGR obtained from the experiments of Valin is the overall FGR, from the intra as well as inter-granular bubbles. Earlier studies had been carried out using the MARGARET model [**?**] to discriminate the intra-granular and inter-granular retained gas. At the end of one cycle irradiation, we get approximately 10% of inter-granular gas. Supposing that the inter-granular gas has been completely released, leads to 55% of the total created gas coming from the grain in the FGR. This would mean that $\frac{0.55}{0.9} = 61\%$ of the intra-granular gas has been released during this annealing test. Secondly, our model uses a planar geometry rather than the actual spherical geometry of the grain. Going from spherical to planar geometry, we get an equivalent value for the FGR as ∼27% as compared to ∼61% FGR from intra-granular bubbles (Appendix B). So, our reference value for FGR from intra-granular bubbles during post-irradiation annealing of UO_2 for 3 hours at 1600°C is 27% for comparison with the calculations in a parallepipedic domain whose length is equal to the grain radius.

We considered a domain of 5510 nm in the x direction, and 120 nm in the y and z direction, including an exterior region of 5 nm. So, the length of the solid (5505 nm) is equal to the mean grain radius in Valin's experiment.

5.2. Conditions of the simulation

Since we are carrying out 3-D calculations, which is closer to reality than 2D, the initialization of the bubble population is conceptually much simpler than in 2D. Using the relation below and the global effective fission yield of 0.3 for gas atoms (Xe+Kr), we estimated the gas generation in our sample to be $189\,mol/m^3$.

$$BU(GWd/t_U) = 3.7384\,10^{-26} \int \dot{F} dt\,(fissions/m^3)$$

We generated bubbles randomly in the domain with bubble radius, R_b equal to 1.7 nm and the volume per atom of gas in the bubbles equal to Ω, the atomic volume of a UO_2 site ($\Omega = 40.9\,10^{-30} m^3$), reaching the desired macroscopic concentration for the gas atoms. The number of bubbles generated was found to be 17933. The grid size was 2 nm. The boundary conditions provided are the periodic boundary condition in the top, bottom, front and back faces and the symmetric boundary condition on the left side of the domain. A "flat bubble" of thickness 5 nm is positioned on the right end of the domain, to simulate the exterior region. Free bubbles and dislocations rebound on the left side, to simulate bubbles or dislocations that would come from the other symmetric side of the grain. A snapshot of the domain including the bubbles is presented in Fig.11. This figure illustrates very clearly how challenging the modeling of individual intra-granular bubbles is with realistic densities ($2.26\,10^{23}\,bubble/m^3$ in this case).

We initialized the domain with 84 dislocations. 42 dislocations were parallel to the y-axis and the other 42 where parallel to the z-axis and these dislocations were randomly distributed within the domain. Within the two groups, half of the dislocations had their direction of climb in the +x direction, while the other half in the -x direction. The total dislocation density was $1.271\,10^{14}\,m/m^3$. Using Nogita's [**?**] correlation ($log_{10}(\rho_d) = 2.2\,10^{-2} \times Bu + 13.8$ with Bu being the burnup in GWd/tU) gives a dislocation density of $1.295\,10^{14}\,m/m^3$, which is close to our dislocation density within 1.8% or about one dislocation in the domain. Fig. 12 shows the initial positions of the dislocations in function of their direction and their +x or -x

possible movement. The value for D^* is not known and is taken as a parameter. D^* is also the diffusion of uranium atoms along the dislocation. The order of magnitude of the D^* that we took is approximately 10^4 times the Uranium diffusion coefficient in the bulk from [**?**] ($D_U = 6.5\,10^{-5}\,exp\left(\frac{-5.6eV}{kT}\right)$), which is plausible for the diffusion along an extended defect. The values of physical conditions used in the analysis are summarized in Table 1.

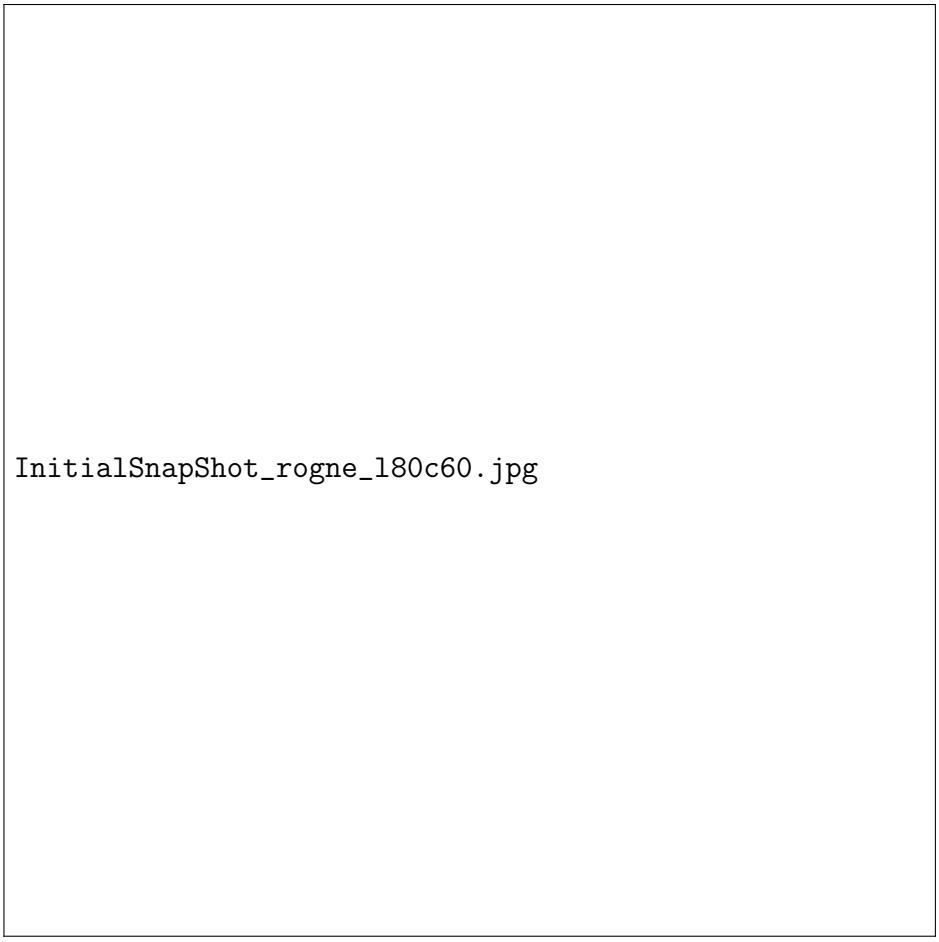

Figure 11: On the top, view of the whole domain, with symmetry condition on the left and free surface on the right. Below, a zoom of the region situated near the free surface is presented to show the high density of individual bubbles.

Figure 12: Initial positions of the dislocations in the domain. (XPd,YPd,0) is the intersection point of a dislocation parallel to the z-axis with the plane z=0. (XPd,0,ZPd) is the intersection point of a dislocation parallel to the y-axis with the plane y=0.

Parameter	Symbol	Value
Solid domain	-	$5505\,nm \times 120\,nm \times 120\,nm$
Length of external region	-	5 nm
Number of bubbles	-	17933
Number of dislocations	-	84
Width of dislocations	w	$1.122 \times \Omega^{1/3}$
Vacancy diffusion coefficient along a dislocation $\times\ x_{v_d}^{eq}$	D^*	$6.9\,10^{-16}\ m^2/\mathrm{s}$
External Pressure	P_{ext}	10^5 Pa
Annealing Temperature	T	1600°C

Table 1: Physical parameters used for the analysis.

BEEP is designed to deal with vacancy diffusion in the bulk, as well as bubble, dislocation and pinned bubble movement and interactions simultaneously. However, for this first real case, we focused on bubble and dislocation coupled behavior only. So, in this case, no vacancy diffusion in the bulk was considered. Random movement of bubbles was activated with a Mikhlin term of 1 (see [**?**] for a discussion on the Mikhlin term) and the same surface diffusion for Uranium atom on the inner surface of the bubble, and same expression for the bubble diffusivity as in [**?**]. The expected behavior was that the bubbles move randomly, coalesce with each other, and/or get pinned on the dislocations, and as pinned bubbles, provide the driving force for dislocation climb. The answer to the question whether this process could lead to a significant FGR, or not, was totally open-ended before the calculation, because, as the dislocations move and the bubbles grow, the driving force diminishes. Therefore, it was not "written in advance", whatever the value for D^*, that the FGR would be significant.

5.3. Results and analysis of the simulation

We tried to carry out the simulation for 3 hours of isothermal annealing. However, the simulation was stopped at 17 min because a bubble became as large as the width of the domain (120 nm), which was incompatible with the periodic limit conditions that we took on the planes perpendicular to the y and z directions. Nevertheless, the obtained results were interesting enough to draw conclusions.

The fission gas release (expressed in percentage of the gas initially present in the solid) reached 46.54% at the end of the calculation, showing that a

fission gas release compatible with the experiment (in this case, even higher) is possible with this mechanism. This is in contrast to the other scenarios tested in [**?**] (random movement of bubbles and movement of bubbles in a vacancy gradient). The FGR evolution is presented in Fig. 13. The analysis of the calculation showed that within the first 15 s the FGR is due to the exit of 26 isolated bubbles, but the remaining FGR is entirely due to pinned bubbles reaching the free surface due to the coupled movement of pinned bubbles and dislocations. The FGR curve presents large steps that correspond to events of arrival of big pinned bubbles at the free surface. Only four dislocations arrived at the free surface but enough gas was gathered in their pinned bubbles to induce the final large FGR. The quantities of gas atoms situated in independent or pinned bubbles respectively is presented in Fig.14.

FGR_30s_2022.pdf

FGR_17min_2022.pdf

Localisation_gas_30s.pdf

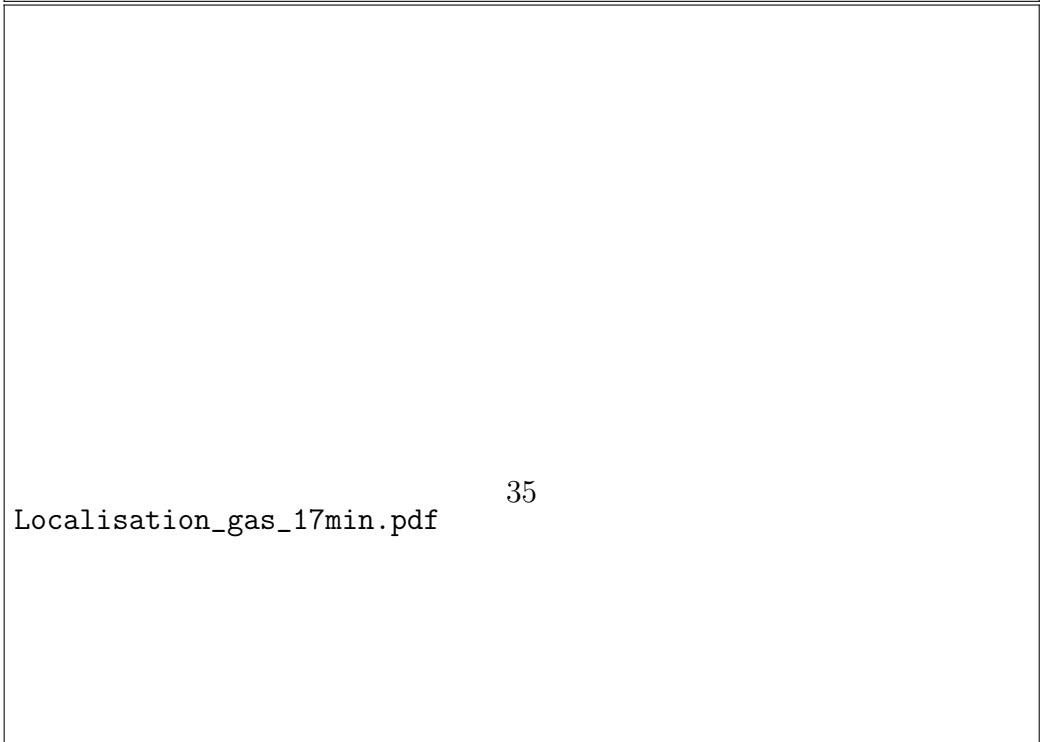

Localisation_gas_17min.pdf

We initialized the dislocations with at least one bubble already pinned on each, choosing the 84 first bubbles of the list (that are randomly placed in the solid domain) and imposing that each of the 84 dislocations intersects the corresponding bubble. It turned out that in fact 96 bubbles (from 17933) were pinned to a dislocation at the beginning of the calculation. The movement of nano-bubbles made them coalesce very quickly. At the same time, most of them got pinned on dislocations as presented in Fig. 15. At the end of the calculation, only 19 bubbles remained, and 18 of them were pinned on dislocations.

BubbleNumbers_30s.pdf

BubbleNumbers_17min.pdf

As expected, globally, the dislocation velocity decreased with time, because as the bubbles grow and the inner pressure of the bubbles decreases, the driving force for the movement ceases. This general trend is verified in Fig. 16. However, the evolution may be very different depending on the particular dislocation considered. Every new pinned bubble on a dislocation boosts its velocity. On the contrary, several dislocations lost a bubble by coalescence with a bubble of another dislocation. Some dislocations lost all their pinned bubbles and stopped.

Dislocation number 31 is an example of a dislocation that loses all its pinned bubbles (see Fig.17). For about 10 minutes, this dislocation evolves with 3 pinned bubbles. Then a first bubble coalesces with a bigger bubble situated on another dislocation, and a few seconds later the two last bubbles coalesce almost simultaneously with another bubble situated on dislocation number 17. Then, without any driving force, dislocation number 31 stops.

Dislocation number 44 is an example of a dislocation that starts towards the left, arrives at the left side of the domain (or grain center), and "rebounds" to simulate a dislocation arriving from the other side of the grain (see Fig.18).

Dislocation number 21 is the one that transports the majority of the FGR (see Fig.19). Contrary to dislocation 31, its velocity does not diminish with time. The reason is that this dislocation encounters several bubbles and gathers their gas, which maintains and even increases the driving force for the movement. Dislocation number 21 finally loses its bubble at 4.66 min by coalescence with the "flat bubble" (or free surface) on the right of the domain, giving rise to a large part of the total FGR.

Fig. 20 and 21 show different snapshots of the vicinity of the free surface. Alignments of bubbles allow the visualization of a few dislocations. On the last view, the bubble that induces the end of the calculation is visible.

Finally, an important characteristic of this evolution is that the gas gradually collects on a few dislocations, the velocity of which is therefore maintained at a fairly high level. Fig. 22 shows the density of dislocations that have pinned bubbles, called "active dislocations" on the figure.


MeanDislocationVelocity_30s.pdf

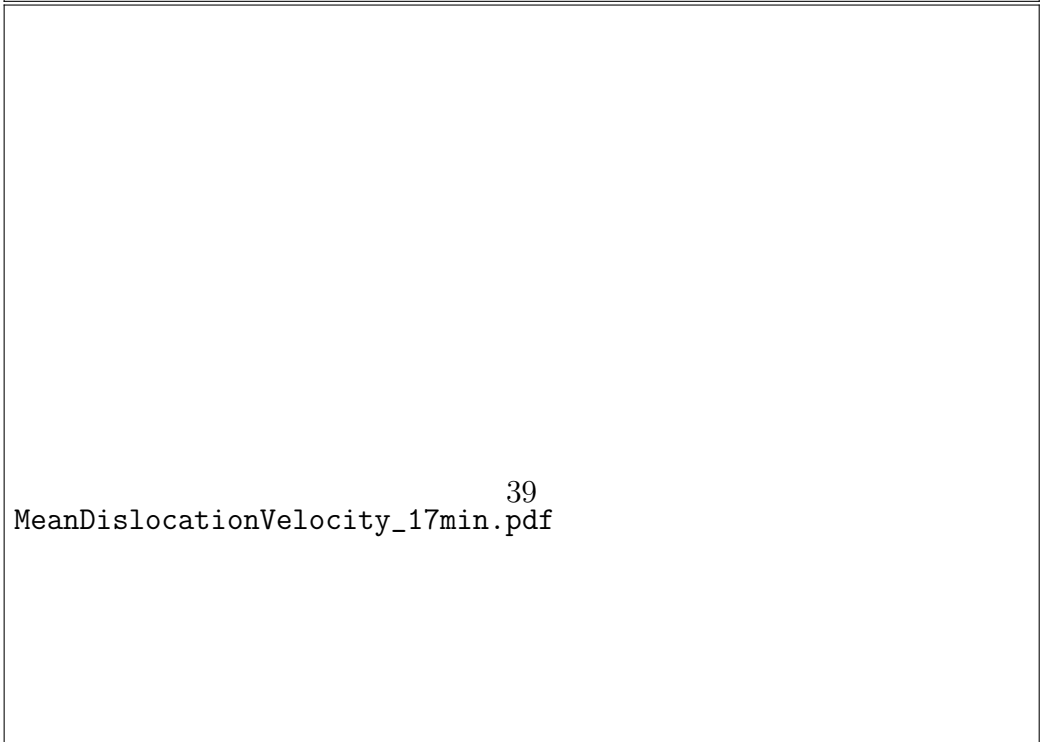
MeanDislocationVelocity_17min.pdf

Figure 17: Evolution of position and pinned bubbles for dislocation number 31

Figure 18: Evolution of position and pinned bubbles for dislocation number 44


Dislocation_n21_X_PinnedBubble.pdf

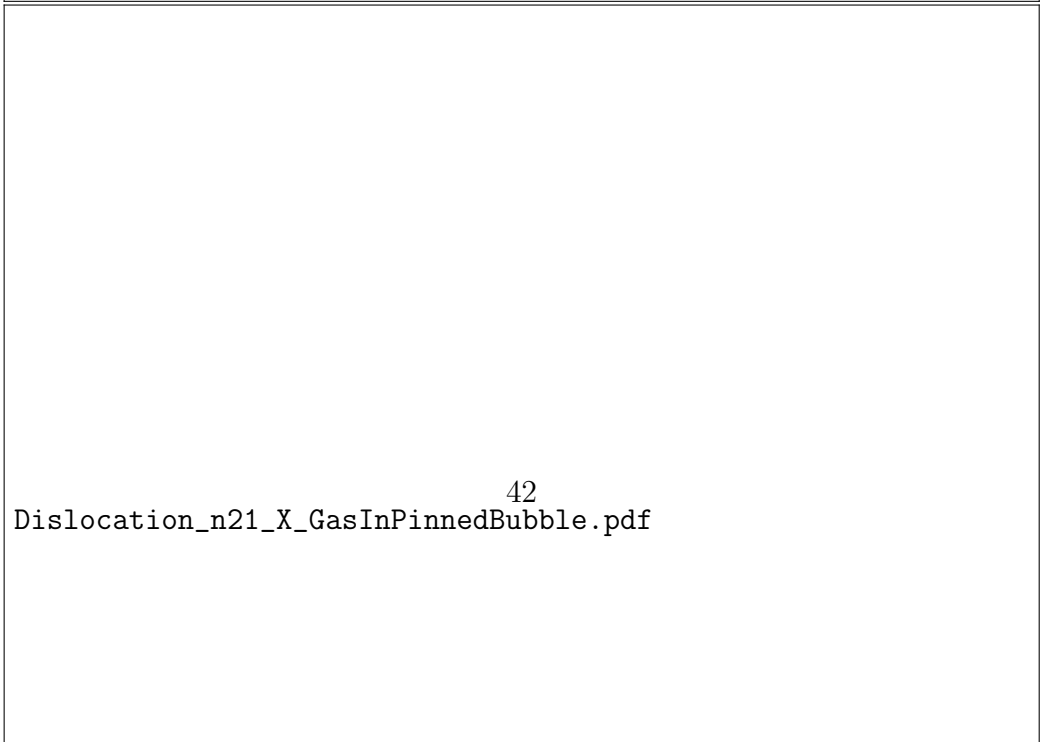
Dislocation_n21_X_GasInPinnedBubble.pdf

dislocfull_002224_zoom_l80c60.jpg

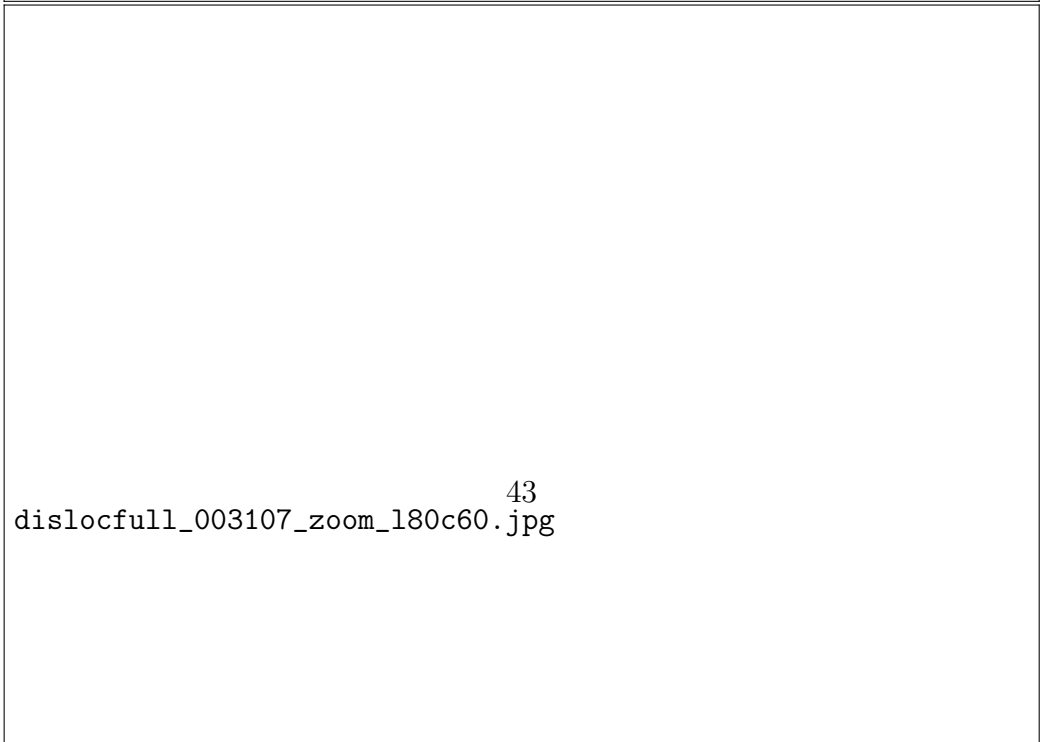

dislocfull_003107_zoom_l80c60.jpg

dislocfull_006440_zoom_l80c60.jpg

dislocfull_007723_zoom_l80c60.jpg

Figure 22: Evolution of the active dislocation density with time.

6. Conclusion and perspectives

There is no clear and shared scenario for gas transport out of grains in annealing conditions. That is why we developed the BEEP model, to study and assess different scenarios for the intra to inter-granular gas transfer in annealing conditions, that is to say, with no possible gas re-solution into the crystal. In preceding papers, bubble movement in a vacancy gradient and random bubble movement were ruled out as efficient enough mechanisms to explain our reference experiment. In this paper, we present a possible new mechanism that leads to directed bubble motion: the dislocation climb due to the presence of pinned over-pressurized bubbles. A first attempt to model this mechanism in the BEEP mesoscale model has been done and the results obtained for the realistic case are encouraging. This first attempt could be improved in many ways.

As a perspective, using the code with both dislocations and vacancy diffusion in the bulk should be the following step. Indeed, even in the case where high gas density bubbles ($V_{at} = \Omega$) would not be mobile (Mikhlin term equal to zero), a slight lowering of gas bubble density by capture of vacancies emitted by already pinned bubbles could make them mobile again. Then short-range mobility of bubbles in a vacancy gradient towards the dislocation could possibly allow them to get pinned anyway.

Besides, bubble balancing on the same dislocation has been adopted in the model for simplicity, but important questions remain unanswered in this regard, and are beyond the scope of BEEP code in its present state of development. Vacancies may be transferred from a bubble to another along the dislocation. In the situation where a dislocation intersects the free surface, or a grain boundary, would its pinned bubbles grow by capture of vacancies arriving from the free surface along the dislocation? Would they lose their driving force to make the dislocation move? Alternatively, would a movement of bubbles in a vacancy gradient along the dislocation towards the free surface be possible and efficient? Secondly, is the thermal resolution of xenon and other fission products from pinned bubbles to the dislocations possible? This would allow a long-range transfer of gas and fission products along the dislocations, and release if the dislocation intersects the free surface. However, this would be contradictory with the fact that all gaseous species are released together [**?**] [**?**], because there is no reason why these different isotopes, or even molecules, would have the same diffusion coefficient along the dislocation core.

We hope to stimulate low scale experimental observation programs and Molecular Dynamic calculations of edge dislocation and over-pressurized bubble interactions. To our knowledge, dislocation dynamics coupled to pinned over-pressurized bubble evolution seems to be a completely unexplored subject, for UO_2. This article indicates that this field may be of crucial interest to understand fully gas species intra to inter-granular transfer, which is the first step of gas release in incidental or accidental conditions.

Acknowledgements

The authors acknowledge AMU, CEA, EDF and Framatome for the financial support of this research conducted in the framework of the PLEIADES project. The authors are also thankful to Gérald Jomard (CEA) for the valuable discussions and encouragement.

Appendix A. Chemical potential in terms of vacancy formation energy

The chemical potential can be expressed in terms of the free energy (F) and the number of vacancies (N_v) as:

$$\mu = \left(\frac{dF}{dN_v} \right) \tag{A.1}$$

Now, consider a system with just the vacancy sites (N_v) and the normal sites (N_s) of a domain that represents the dislocation region (Fig.A.23).

The total number of sites = $N_v + N_s$ = constant, which gives:

$$dN_s = -dN_v \tag{A.2}$$

From Olander [**?** , Eq.1.25 , pg5], we get the expression for the free energy as:

$$F = -kTln(Z)$$

where k is the Boltzmann constant, T is the temperature (K) and Z is the partition function of the defected lattice. The partition function Z can be expressed as a product of the three terms, Z1, Z2 and Z3, which are:

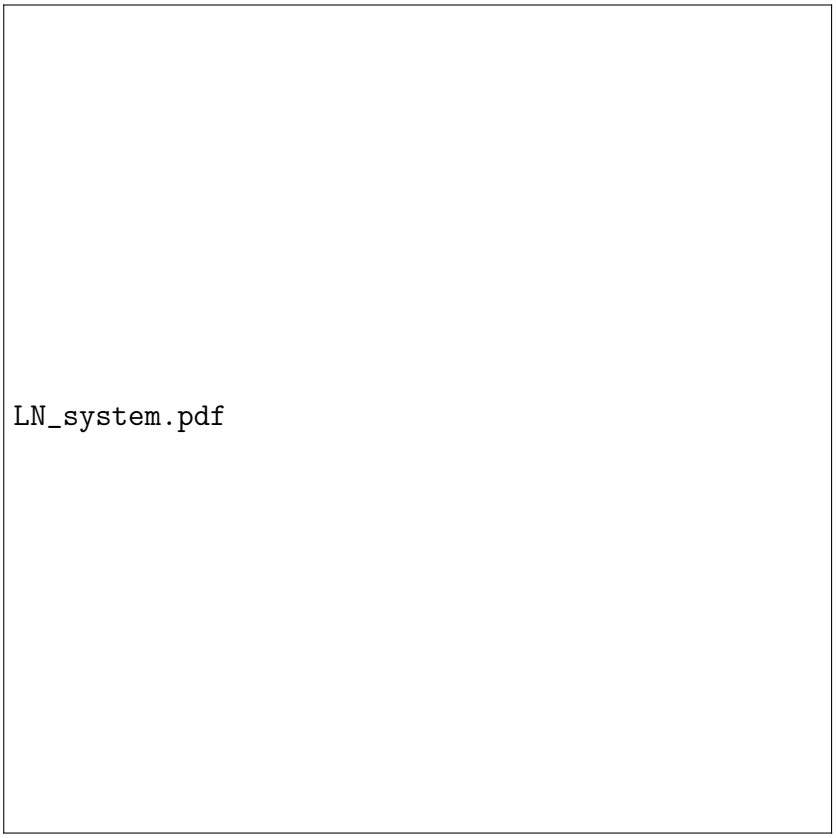

Figure A.23: Box containing vacancies and normal (crystal atom) sites.

- Z1: involves the energies of the defects at zero Kelvin. So for the system presented above

$$Z1 = exp\left(-N_s\frac{E_0}{kT} - N_v\frac{E_v}{kT}\right)$$

  where E_0 and E_v are the energies of the crystal atom and the vacancy site in the lattice at 0 K.

- Z2: represents the number of ways to distribute a particular site among all the sites available. For the system here

$$Z2 = \frac{(N_s + N_v)!}{N_v!N_s!}$$

- Z3: accounts for the vibration modes of all the atoms. The changes in Z3 are neglected in the following.

From the above expressions, we can derive:

$$ln(Z1) = -N_s\frac{E_0}{kT} - N_v\frac{E_v}{kT}$$

and using the Stirling formula, ln(N!) = N ln(N) - N, we derive:

$$ln(Z2) = (N_s + N_v)ln(N_s + N_v) - N_s ln(N_s) - N_v ln(N_v)$$

For the derivation, we use the relation between the total and partial derivatives. From Eq.A.2:

$$\frac{d}{dN_v} = \frac{\partial}{\partial N_v}\frac{\partial N_v}{\partial N_v} + \frac{\partial}{\partial N_s}\frac{\partial N_s}{\partial N_s} = \frac{\partial}{\partial N_v} - \frac{\partial}{\partial N_s}$$

Now, the chemical potential, from Eq.A.1

$$\begin{aligned}\mu &= \left(\frac{dF}{dN_v}\right) = -kT\left[\frac{d}{dN_v}ln(Z1) + \frac{d}{dN_v}ln(Z2)\right] \\ &= -kT\left[-\frac{(E_v - E_0)}{kT} - ln\frac{N_v}{(N_s + N_v)} + \underbrace{ln\frac{N_s}{(N_s + N_v)}}_{\approx 0}\right]\end{aligned}$$

So, we get

$$\mu = (E_v - E_0) + kTln\frac{N_v}{(N_s + N_v)}$$

If we define $x_{v_d} = \frac{N_v}{N_s+N_v}$ as the local concentration of vacancies in the dislocation region (in fraction/site), we get the relation for chemical potential as:

$$\mu = (E_v - E_0) + kTln(x_{v_d})$$

$(E_v - E_0)$ is the formation of a vacancy in the dislocation region, denoted as E_{v_d} in section 2.1. It may be obtained by DFT or MD calculations comparing the energies of two boxes. The first one contains a dislocation with a vacancy at its vicinity (dislocation region). The other one contains the same dislocation without the vacancy, such that:

$$E_{v_d} = (E_v - E_0) = E_{Box1} - E_{Box2}$$

Appendix B. Target value of FGR (From spherical to planar geometry)

Following the idea of Evans[**?**], if the spherical grain is divided into shells and the FGR comes from the outermost shell of the grain, then a sphere of radius R_{ext} would be depleted of gas bubbles up to the radius R_1 (Fig.B.24).

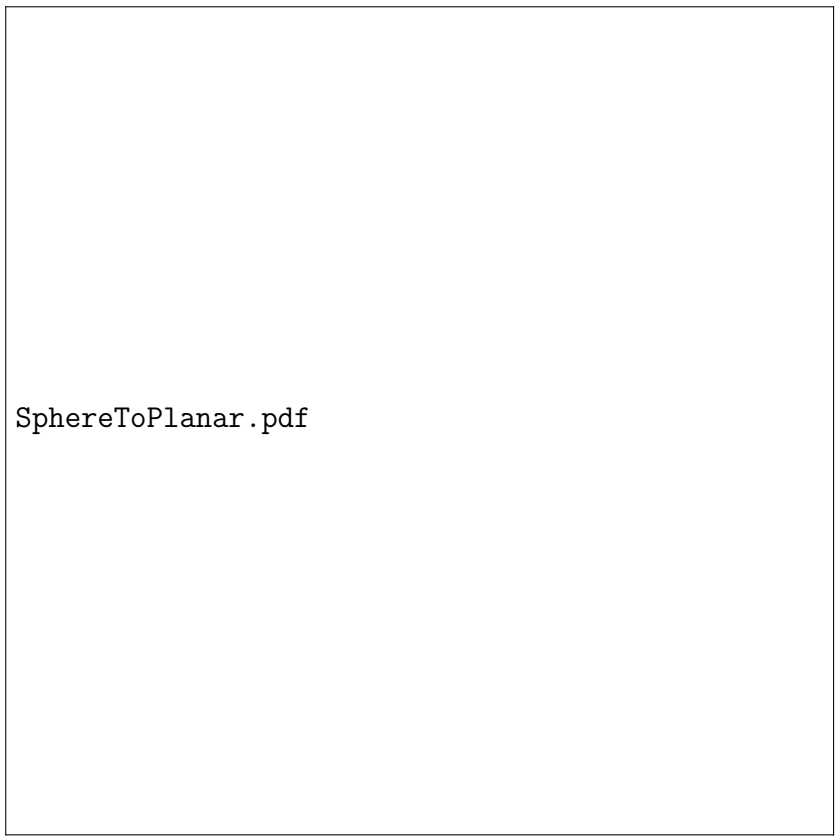

Figure B.24: Target value of FGR from spherical to planar geometry.

The volume of FGR from the sphere can be represented as:

$$\frac{4}{3}\pi(R_{ext}^3 - R_1^3)$$

This volume represents 61% of total gas release, so

$$\frac{4}{3}\pi(R_{ext}^3 - R_1^3) = 0.61 * \frac{4}{3}\pi R_{ext}^3$$

which gives us the fraction of gas retained in the sphere as:

$$\frac{R_1}{R_{ext}} = 0.7306$$

Now, if we consider the same R_1 and R_{ext} in a planar geometry, then the fraction of gas released would be given by $1 - \frac{R_1}{R_{ext}}$ and this value is 0.2694.

So, for a 61% FGR in a spherical geometry, we can roughly have an equivalent FGR of $\sim$ 27% in the planar geometry.

References